Spectral density functions for polyacetylene within the Peierls - Hubbard model

1996 J. Phys.: Condens. Matter 8 8995

(http://iopscience.iop.org/0953-8984/8/46/006)

J. Phys.: Condens. Matter **8** (1996) 8995–9009. Printed in the UK

Spectral density functions for polyacetylene within the Peierls–Hubbard model

D Góra and K Rościszewski

Institute of Physics, Jagiellonian University, Reymonta 4, 30-059 Kraków, Poland

Received 8 July 1996

Abstract. A Peierls–Hubbard Hamiltonian suitable for the description of polyacetylene electronic structure is studied. We employ the Lanczos method to calculate the ground-state properties and single-particle spectral density functions appropriate for the description of the photoemission and the inverse photoemission spectra.

The data obtained confirm that the dimerized polyacetylene is more stable than an undimerized one and elucidate how the Coulomb and the electron–phonon interactions open up a charge-transfer gap near the Fermi level. In particular we found that the value of the gap increases when the electron–phonon interaction is switched on.

1. Introduction

Polyacetylene (PA) is one of the most famous polymers. This is due in part to the fact that PA is the simplest conjugated organic polymer, and thus a comparison of various theoretical approaches with experiment is relatively easy [1]. The shortcomings of applying simple theoretical approaches like local density approximation or Hartree–Fock approximation to systems like PA are understood relatively well [2]. In order to obtain correct values of the band gaps, quasiparticles, and even simple ground-state properties it is necessary to include electron correlation effects, i.e. all the effects of electron–electron interactions which are not included in the Hartree–Fock calculations. Unfortunately, such calculations for infinite systems are difficult and costly (compare [2–6]).

The first good quality *ab initio* correlation calculations for infinite one-dimensional PA were reported in [7]. The dependence of the ground-state energy on the dimerization was analysed. It was claimed that the correlation effects are responsible for the observed large dimerization. The dimerization problem was also studied (using the Lanczos method) in references [8, 9]. Then the calculation of the charge-transfer gap was performed in [9].

On the other hand, the phase diagram of extended Hubbard-type one-dimensional models well suitable for the description of PA was investigated using various techniques such as the Hartree–Fock functional integral formalism, quantum Monte Carlo simulation, and the renormalization group and Lanczos methods [10–17].

In the present short note we would like to supplement all of the theoretical data on PA by computation of spectral density functions. In addition we will pay attention to the problem of the nature of the charge-transfer gap and to the problem of dimerization. Here the correlation effects must be treated properly—most of the simple analytical approximations used for these purposes are simply uncontrollable. Therefore we will use the exact (no approximations)

0953-8984/96/468995+15$19.50

Lanczos method applied to small clusters. Such an approach yields deviations from infinite-system data but the deviations are well understood. That is, the trends in finite-size effects can be inferred from calculations done on several clusters of different sizes.

Let us now consider, in detail, the problem of which model is appropriate for the proper description of PA. PA is a linear polymer which consists of CH units forming a quasi-one-dimensional lattice. Three of the four carbon valence electrons participate in σ-bonds, while one electron participates in the π-bond (sp^2 hybridization). Electronic energies of σ-bonds are at relatively deep levels. The interesting low-energy physical behaviour of PA can be accounted for by taking into account the effective Hamiltonian describing the π-electrons alone. The competition between the lowering of the electronic energy caused the formation of a conjugated single–double-bond structure and the increase of the elastic energy of the polymer (caused by distortion) leads to an equilibrium bond-length modulation (dimerization). The simplest Hamiltonian capable of modelling this situation is the Su–Schrieffer–Heeger (SSH) Hamiltonian [18]. This is a model based on an effective free electron plus 'static' phonons plus the possibility of dimerization. Correlation effects are non-existent. When the SSH model is extended (by adding Coulomb interactions between electrons) we obtain the Peierls Hubbard Hamiltonian [8, 19]:

$$H = \sum_{l,\sigma} t_{l,l+1}(c^+_{l,\sigma}c_{l+1,\sigma} + \mathrm{HC}) + U\sum_{l} n_{l,\uparrow}n_{l,\downarrow} + V\sum_{l} n_l n_{l+1} + 2NK\zeta^2 - \mu\sum_{l} n_l. \tag{1}$$

Here $c^+_{l,\sigma}$ and $c_{l,\sigma}$ are fermion creation and annihilation operators of the π-electron with spin σ on site l, and $n_{l,\sigma} = c^+_{l,\sigma}c_{l,\sigma}$ is the corresponding particle number operator. The first term of (1) represents kinetic energy of the electrons, i.e., the hopping between neighbouring sites ($t_{l,l+1} = t_1$ or t_2; $t_1 = t_0 + 2\alpha\zeta$ or $t_2 = t_0 - 2\alpha\zeta$ are the hopping integrals for double and single π-bonds). The second term (U) is the on-site Coulomb repulsion while the third one (V) corresponds to nearest-neighbour Coulomb interaction. The fourth term describes the elastic energy: ζ is dimerization and K, α are electron–phonon constants. The last term is the chemical potential. The Hamiltonian (1) is invariant under particle–hole transformation for $\mu = 2V + U/2$, i.e. for a half-filled band. This is true for the undimerized case, i.e. for $\zeta = 0$. The values of the (t, U, V) parameters determine the type of the ground state [8, 15, 17]. Three special cases, $t \gg U, V$ (free fermionic), $U \gg t, V$ (Mott–Hubbard) and $V \gg t, U$ (the charge-density wave), are of special interest. For $U \gg t$ the ground state has singly occupied sites and Hamiltonian (1) reduces to an effective antiferromagnetic (AFM) Heisenberg Hamiltonian. For $V \gg t, U$ the ground state has alternate empty and doubly occupied sites [20]. It was found that on the U–V diagram charge-density-wave (CDW) and spin-density-wave (SDW) phases are separated by the transition line $U = 2V$ [17] on which the amplitude of dimerization reaches a maximum [8].

2. Computational details

We study the clusters of $N = 6, 8, 10$ sites. A crucial point is the selection of the values of the parameters for the Hamiltonian and choosing the appropriate boundary conditions. Here we use $t_0 = -2.5$ eV, $\alpha = 40$ meV pm^{-1}, $U = -6.25$ eV, $V = U/2 = 3.15$ eV and the experimental value $\zeta = 2.6$ pm [21] (see table 1; set V parameters). In table 1 we present other sets of parameters which merit some additional study.

Some comments on table 1 are appropriate at this point. The values of the parameters entering the model Hamiltonian (1) are not precisely known for PA. For dimerization we can take the experimental value $\xi = 2.6$ pm [21]. If one wished to accept the parameters from

Table 1. The sets of model parameters.

Set:	I	II	III	IV	V
t_1 (eV)	−2.5	−2.708	−2.5	−2.5	−2.708
t_2 (eV)	−2.5	−2.292	−2.5	−2.5	−2.292
U (eV)	0.0	0.0	6.25	6.25	6.25
V (eV)	0.0	0.0	0.0	3.125	3.125
ζ (pm)	0.0	2.6	0.0	0.0	2.6
μ (eV)	0.0	0.0	3.125	9.375	9.375
K (10^{-3} eV pm^{-1})	0.0	3.132	0.0	0.0	3.132

references [1, 7] then: $t_0 = -2.5$ eV and $\alpha = 40$ meV pm^{-1} giving $t_1 = -2.708$ eV, $t_2 = -2.292$ eV. The electron–electron interactions are described by $U = 11.5$ eV, $V = 2.4$ eV. The very large value of U ($U > -4.0t_0$) is usually not accepted as the correct one for PA. Experimentalists favour a much lower value: $-1.5t_0 < U < -3.5t_0$ [22–24], arguing that large values of U [7] are bare values, and that the effective U that one should use is much lower (probably due to some screening effects). For V the estimate is $-0.5t_0 < V < -1.5t_0$ [22, 23]. Therefore, in the following, we will consider as the most probable the parameters $U = -2.5t_0 = 6.25$ eV, $\alpha = 40$ meV pm^{-1} [22, 23, 24] and $V = U/2 = 3.125$ eV. Note that the value of V set arbitrarily to one half of U corresponds to maximal possible dimerization, as found in small-cluster calculations [8]. These are the set V parameters. Set IV is identical to set V with the exception that the dimerization and electron–phonon interaction are omitted. Set III is a simplified version of set IV (without V-interaction). We consider these model parameters following reference [24]. The parameters of set II are simply SSH Hamiltonian parameters [18]. Finally the free-electron case—set I—corresponds to set II when the dimerization and electron–phonon interaction are switched off.

The importance of imposing the proper boundary conditions in small-cluster calculations was recognized by several authors [8, 15, 25]. That is, there is a subtle difference between the chains with $N = 4m$ and $N = 4m + 2$ sites. In order to approximate the infinite chain by finite rings with the states at the Fermi level, cyclic boundary conditions are the most suitable in the first case, whereas anticyclic boundary conditions have to be imposed in the second one. More detailed discussion is given in references [9, 15, 25].

Therefore we use modified periodic boundary conditions (MPBC), i.e., the true periodic boundary conditions (PBC) are appropriate for rings with eight sites while for rings with six or ten sites antiperiodic boundary conditions (ABC) are appropriate [8, 9, 15, 25]. Note that for PBC we have used $t_{N,N+1} = t_{N,1} = t_2$ and $V_{N,N+1} = V_{N,1} = V$ and for ABC the sign of the hopping integral is changed: $t_{N,N+1} = t_{N,1} = -t_2$ [9].

The Lanczos method is an excellent one for obtaining low-lying eigenvalues and ground-state properties for a small cluster. It is described in detail in numerous papers and textbooks [20, 26–29]. The Lanczos method allows for the computation of spectral density functions by the method of continued-fraction expansion [20, 30–32].

For small clusters of $N = 6, 8, 10$ sites the actual computations were fast and could be completed on personal computers or small work-stations. Applying the Lanczos method we calculate:

(i) the ground state E_0^N and lowest excited states;
(ii) the occupations numbers $\langle n_{l,\sigma}\rangle$;
(iii) the spin–spin correlation functions $\langle S_l^z S_l^z\rangle$;
(iv) the single-particle densities of states for photoemission and inverse photoemission.

Considering the momentum-integrated one-particle spectral density function, we define

$$N^A(\omega) = \frac{1}{N}\sum_{l,n,\sigma} |\langle\psi_n^{N+1}|c_{l,\sigma}^+|\psi_0^N\rangle|^2\delta(\omega - (E_n^{N+1} - E_0^N)) \tag{2}$$

(corresponding to the addition of an electron to a half-filled system or to inverse photoemission) and

$$N^E(\omega) = \frac{1}{N}\sum_{l,n,\sigma} |\langle\psi_n^{N-1}|c_{l,\sigma}|\psi_0^N\rangle|^2\delta(\omega - (E_n^{N-1} - E_0^N)) \tag{3}$$

(corresponding to the removal of an electron from a half-filled system or to photoemission). Here E_n^N and $|\psi_n^N\rangle$ are the nth excited eigenvalue and eigenvector of the N-site system respectively; $n = 0$ denotes the ground state.

The one-particle spectral function $N^E(\omega)$ connected with photoemission and $N^A(\omega)$ connected with inverse photoemission can be related to the following Green's functions [2]:

$$G_{l,\sigma}^E(\omega) = \langle\psi_0^N|c_{l,\sigma}^+\frac{1}{\omega + E_0^N - H + \mathrm{i}\eta}c_{l,\sigma}|\psi_0^N\rangle \tag{4}$$

$$G_{l,\sigma}^A(\omega) = \langle\psi_0^N|c_{l,\sigma}\frac{1}{\omega + E_0^N - H + \mathrm{i}\eta}c_{l,\sigma}^+|\psi_0^N\rangle. \tag{5}$$

The relation between total density of states $N_\sigma^A(\omega)$ and $G_{l,\sigma}^A(\omega)$ is easily obtained as [29]

$$N^A(\omega) = \sum_\sigma N_\sigma^A(\omega) \tag{6}$$

where

$$N_\sigma^A(\omega) = \frac{1}{N}\sum_{l,n} |\langle\psi_n^{N+1}|c_{l,\sigma}^+|\psi_0^N\rangle|^2\delta(\omega - (E_n^{N+1} - E_0^N)) = -\frac{1}{\pi N}\lim_{\eta\to 0}\sum_{l=1}^N \mathrm{Im}\, G_{l,\sigma}^A(\omega). \tag{7}$$

Here η is a small positive number. (In practice, during the following computations, we set $\eta = 0.1$ eV. This gives an artificial width to the delta functions.) The chemical potential μ can be defined in a standard way or equivalently as follows: $N^A(\omega) = 0$ for $\omega < \mu$; $N^E(-\omega) = 0$ for $\omega > \mu$.

3. Results

3.1. The ground state

To give an example of the results obtained we present table 2.

According to the theorem given by Lieb and Mattis [33], in one dimension the total spin of the ground-state wave function of an infinite chain is zero. This is in agreement with our results. The charge excitation gap for PA can be obtained from small-cluster data as [9, 15, 20, 34]

$$E_{gap} = \lim_{N\to\infty} E_{gap}^N \tag{8}$$

$$E_{gap}^N = E_0^N(n_\uparrow, n_\downarrow + 1) - 2E_0^N(n_\uparrow, n_\downarrow) + E_0^N(n_\uparrow, n_\downarrow - 1) \tag{9}$$

Table 2. Numerical results for $N = 10$.

Set:	I	II	III	IV	V
E_0^N (eV)	−30.7627	−31.269	−50.135	−86.029	−86.600
$\langle\|n_{l,\sigma}\|\rangle$	0.5	0.5	0.5	0.5	0.5
$\langle\|S_l^z S_l^z\|\rangle$	0.358	0.375	0.535	0.485	0.436
$\langle\|S_{total}^2\|\rangle$	0.0	0.0	0.0	0.0	0.0

where $E_0^N(n_\uparrow, n_\downarrow)$, $E_0^N(n_\uparrow, n_\downarrow + 1)$, $E_0^N(n_\uparrow, n_\downarrow - 1)$ are ground-state energies for systems with $(n_\uparrow, n_\downarrow)$, $(n_\uparrow, n_\downarrow + 1)$ and $(n_\uparrow, n_\downarrow - 1)$ up and down electrons, respectively.

E_{gap} is an essential quantity for the indication of metal–insulator phase transition. A system is insulating if the gap is finite. In our case, the charge excitation gaps, E_{gap}^N, calculated using set V parameters are: $E_{gap}^6 = 3.62$ eV, $E_{gap}^8 = 3.09$ eV and $E_{gap}^{10} = 2.77$ eV. It is well known [9, 15, 25, 35] that E_{gap}^N varies roughly linearly with $1/N$, so extrapolation to an infinite system is possible [20, 36]. (Better extrapolation schemes than the $1/N$ linear dependence do exist when the data for many different $N = 6, 8, 10, 12, \ldots$ are available—compare [15].) We have obtained the value $E_{gap} = 1.55$ eV.

For set I/set II parameters the ground state is metallic/semimetallic ($E_{gap} \simeq 0$, $\langle|S_i^2|\rangle = 0.375$). The ground-state energy is [1, 18]

$$E_0(\zeta) = -N\frac{4t_0}{\pi}E(1 - Z^2) + \frac{4t_0 Z^2}{2\alpha^2} \tag{10}$$

where $E(1 - Z^2)$ is the complete elliptic integral of the second kind and $Z = 2\alpha\zeta/t_0$. For set III (the Hubbard Hamiltonian) an exact solution in one dimension (based on the Bethe *ansatz*) was found by Lieb and Wu [34]. The ground-state energy is

$$E_0 = -4\int_0^\infty \frac{J_0(\omega)J_1(\omega)}{\omega(1 + \exp(0.5\omega U))}\,\mathrm{d}\omega \tag{11}$$

where $J_0(\omega)$ and $J_1(\omega)$ are Bessel functions. For set IV (when $U = 2V$), the system is in the SDW phase [19, 8, 15] and the ground-state energy in second-order perturbation theory is [37]

$$E_0^N \simeq -N\left(V + \frac{4t^2 \ln 2}{U - V}\right). \tag{12}$$

At half-filling for very large U there should be no doubly occupied sites. An effective Hamiltonian for PA becomes in this case the Hamiltonian for the Heisenberg antiferromagnet with the exchange integral $J_{eff} = t^2/(U - V)$ [20] ($J_{eff} = 4$ eV for set IV). For set V the ground-state energy should have the following expansion [38]:

$$E_0^N = e_0 + \left[e_1 + e_2\,\ln\left(\frac{4}{|z|}\right) + e_3\,\ln^2\left(\frac{4}{|z|}\right)\right]z^2 \tag{13}$$

valid for a small dimerization only. For $4\mathrm{e}^{-z-\pi t/V} \leqslant z \ll 1$ the parameter z is related to the dimerization by

$$\zeta(z) = \left[t + \frac{2V}{\pi} - \frac{V}{\pi}\ln\left(\frac{4}{|z|}\right)\right]\frac{z}{2\alpha}. \tag{14}$$

The coefficients e_i are analytic functions of the model parameters (see [38], and also appendix A). Our numerical results for all sets of parameters agree within a few per cent with theoretical values following from equations (10)–(13). An additional important finding

is that the ground-state energy for a dimerized system is lower than that for a non-dimerized one, which confirms the results of references [7–9]. Let us recall that the driving force for dimerization is provided by electron correlations. The stronger the correlations (the larger U), the more stable the dimerized state. We also recall that at the line $V = U/2$ the dimerization is at its maximum [8].

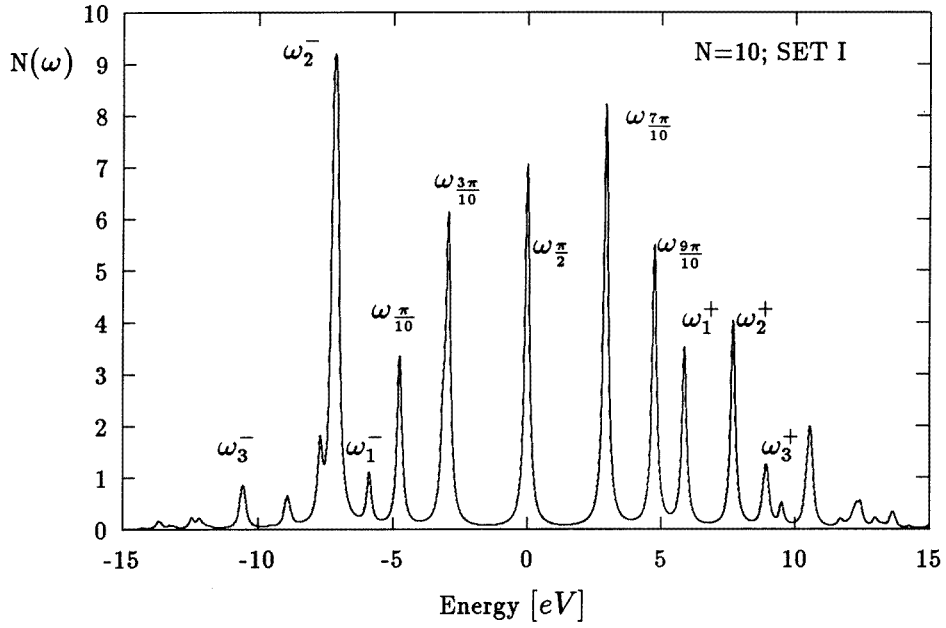

Figure 1. The one-particle spectral function $N(\omega) = N^E(-\omega) + N^A(\omega)$ for a 10-site cluster expressed in arbitrary units (set I parameters, ABC). The energy is measured with respect to the ground-state energy E_0^{10}. The chemical potential $\mu = 0$. The peak labels corresponding to different k-values were assigned using formula (17). Other peaks correspond to $\omega_1^{\pm} = \pm 2\omega_{-3\pi/10}$, $\omega_2^{\pm} = \pm(\omega_{-3\pi/10} + \omega_{-\pi/10})$, $\omega_3^{\pm} = \pm 3\omega_{-3\pi/10}$.

3.2. The one-particle density function

For the sake of completeness, we start by calculating the one-particle spectral density function $N(\omega) = N^A(\omega) + N^E(-\omega)$ using set I parameters. (This will turn out to be useful when we discuss spectral density functions in the Hartree–Fock approximation for the other sets.) In figure 1 we show $N(\omega)$ versus ω (10-site cluster, ABC boundary conditions). This function has a periodic structure. For set I parameters

$$H = t_0 \sum_{l,\sigma} (c^+_{l,\sigma} c_{l+1,\sigma} + \text{HC}). \tag{15}$$

The kinetic energy is diagonal in the momentum representation [2]:

$$H = \sum_{k,\sigma} E_k c^+_{k,\sigma} c_{k,\sigma} \tag{16}$$

where

$$E_k = 2t_0 \cos k \tag{17}$$

and the wave vector $k = 2\pi j/N - \phi/N$; $j = -N/2, \ldots, N/2$. The phases $\phi = 0$ and $\phi = \pi$ correspond to PBC and ABC, respectively. The Hamiltonian (15) describes the system of non-interacting electrons for which the density of states for momentum q and for ω is defined as [2]

$$N_\sigma^A(q,\omega) = -\frac{1}{\pi}\lim_{\eta\to 0}\mathrm{Im}\left(\langle\psi_0^N|c_{q,\sigma}\frac{1}{\omega + E_0^N - H + \mathrm{i}\eta}c_{q,\sigma}^+|\psi_0^N\rangle\right) \tag{18}$$

$$N_\sigma^E(q,\omega) = \frac{1}{\pi}\lim_{\eta\to 0}\mathrm{Im}\left(\langle\psi_0^N|c_{q,\sigma}^+|\frac{1}{\omega + E_0^N - H + \mathrm{i}\eta}c_{q,\sigma}|\psi_0^N\rangle\right). \tag{19}$$

Using the identities

$$1 = \sum_k |\psi_k^{N+1}\rangle\langle\psi_k^{N+1}| \tag{20}$$

where k denotes the wave vector and $|\psi_k^{N+1}\rangle$ is the Bloch wave function and

$$\delta(x) = \lim_{\eta\to 0}\frac{\eta^2}{\pi(x^2+\eta^2)} \tag{21}$$

we can convert equation (18) into the form

$$N_\sigma^A(q,\omega) = \sum_k |\langle\psi_k^{N+1}|c_{q,\sigma}^+|\psi_0^N\rangle|^2\delta(\omega - (E_k - E_0^N)). \tag{22}$$

In this case the local density of states $N^A(\omega)$ is

$$\begin{aligned} N^A(\omega) &= \frac{1}{N}\sum_{q,k,\sigma}|\langle\psi_k^{N+1}|c_{q,\sigma}^+|\psi_0^N\rangle|^2\delta(\omega - (E_k - E_0^N)) \\ &= \sum_{k,\sigma}(1 - \langle n_\sigma\rangle)\delta(\omega - (E_k - E_0^N)) \end{aligned} \tag{23}$$

where $\langle n_\sigma\rangle = (1/N)\sum_q\langle n_{q,\sigma}\rangle$. In the same way we obtain $N^E(\omega)$. Because $\langle n_\sigma\rangle = 0.5$ the total density of states $N(\omega)$ becomes

$$N(\omega) = N^A(\omega) + N^E(-\omega) = \sum_k[\delta(\omega - (E_k - E_0^N)) + \delta(\omega + (E_k - E_0^N))]. \tag{24}$$

If energy is measured with respect to the ground-state energy then the peaks of the spectral function $N(\omega)$ are located at

$$\omega = \pm E_k. \tag{25}$$

The negative and positive signs in (25) refer to valence and conduction bands.

For $N = 10$, from equation (17) we have obtained: $\omega = 0$ eV for $k = \pm\pi/2$, $\omega = \pm 2.94$ eV for $k = \pm 3\pi/10$ and $k = \pm 7\pi/10$, and $\omega = \pm 4.76$ eV for $k = \pm\pi/10$ and $k = \pm 9\pi/10$, where the signs $\pm$ correspond to $N^A(\omega)$ and $N^E(\omega)$, respectively. This is shown in figure 1. The one-particle spectrum has a symmetry with respect to the reflection $\omega \to (-\omega)$. This is caused by particle–hole symmetry. Single-mode peaks are identified by using labels ω_k, that is: $\omega_{9\pi/10}$, $\omega_{7\pi/10}$, $\omega_{\pi/2}$, $\omega_{3\pi/10}$.

Other peaks correspond to $\omega_1^\pm = \pm 2\omega_{-3\pi/10}$, $\omega_2^\pm = \pm(\omega_{-3\pi/10} + \omega_{-\pi/10})$, $\omega_3^\pm = \pm 3\omega_{-3\pi/10}$. It was shown in [39, 40] that the density of states becomes Gaussian in the limit of infinite dimension. Looking at figure 1 we note the beginning of such a tendency.

For set II the only difference in comparison to the set I results is that we should replace E_k with E_k^D [1, 18]:

$$E_k^D = [t_1^2 + 2t_1t_2\cos(2k) + t_2^2]^{1/2} \tag{26}$$

where $t_1 = t_0 + 2\alpha\zeta$, $t_2 = t_0 - 2\alpha\zeta$. The spectral function $N(\omega)$ is

$$N(\omega) = \sum_k [\delta(\omega - (E_k^D - E_0^{N,D})) + \delta(\omega + (E_k^D - E_0^{N,D}))] \tag{27}$$

where $E_0^{N,D}$ is the ground state in the case of dimerization. The positions of the peaks for the $N = 10$ cluster are given by: $\omega = 2\alpha\zeta = \pm 0.42$ for $k = -\pi/2$, $\omega = \pm 2.94$ for $k = \pm 3\pi/10$ and $k = \pm 7\pi/10$, and $\omega = \pm 4.76$ for $k = \pm 9\pi/10$ and $k = \pm\pi/10$.

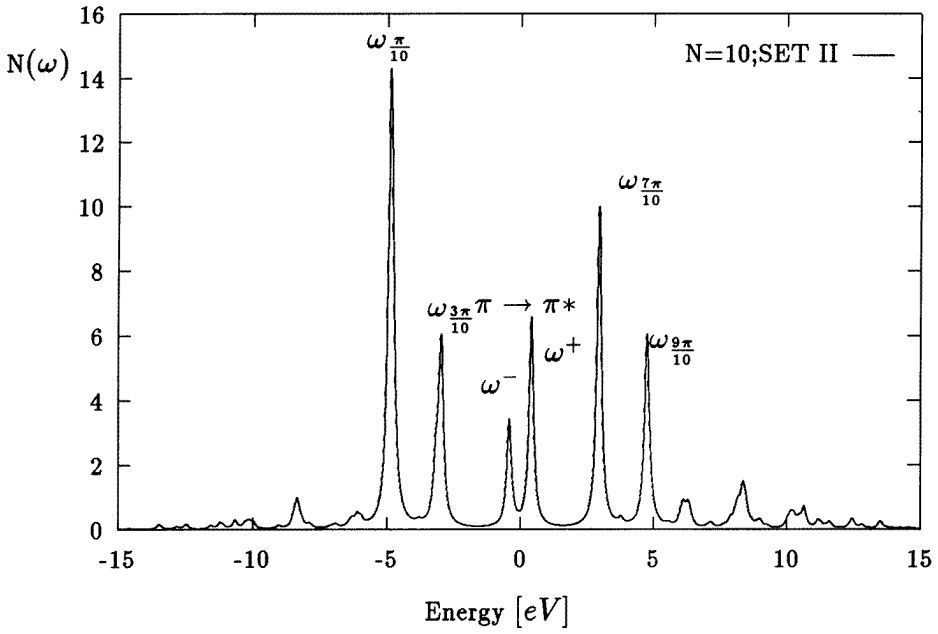

Figure 2. The one-particle spectral function $N(\omega) = N^E(-\omega) + N^A(\omega)$ for a 10-site cluster expressed in arbitrary units (set II parameters, ABC). The chemical potential (defined as $0.5E_{gap}$) is $\mu = 0.42$ eV. We see a $\pi \rightarrow \pi^*$ charge-transfer-type gap corresponding to a transition from a bonding ω^--state to an antibonding ω^+-state. Note that the band width is $W = 4t_0$.

The agreement of infinite-system values with the corresponding small-cluster data is very good (figure 2). In the vicinity of $\omega = 0$ we see a charge-transfer-type gap (labelled $\pi \rightarrow \pi^*$) corresponding to a transition from a bonding ω^--state to an antibonding ω^+-state [41, 42]. We find that dimerization opens the energy gap near the Fermi surface (the Peierls transition). We can estimate E_{gap} from figure 2 ($E_{gap}^{10} = \omega^+ - \omega^- = 0.84$ eV). Note that $E_{gap}^6 = E_{gap}^8 = E_{gap}^{10} = 0.84$ eV does not agree with the experimental value $E_{gap}^{exp} \approx 1.8$ eV [1, 43], which indicates that effective Hamiltonian (1) with set II parameters does not describe the PA very well. We also see that large dominant structures at energies $|\omega| < 5 - 6$ eV correspond to the band width $W = 4t_0$.

For set III parameters, equation (1) reduces to the form

$$H = \sum_{l,\sigma} t_0 (c_{l,\sigma}^+ c_{l+1,\sigma} + \text{HC}) + U \sum_l n_{l,\uparrow} n_{l,\downarrow} - \mu \sum_l n_l. \tag{28}$$

In the Hartree–Fock (HF) approximation [2]

$$H \simeq \sum_{k,\sigma} (E_k^N + U\langle n_\sigma \rangle - \mu) c_{k,\sigma}^+ c_{k,\sigma}. \tag{29}$$

The corresponding approximate Green's function is of the form [2]

$$G_{\sigma}^{HF,A}(k,\omega) = \frac{1}{\omega + E_0^N - E_k - U\langle n_\sigma\rangle - \mu + \mathrm{i}\eta}. \tag{30}$$

The poles are located at

$$\omega = E_k + U\langle n_\sigma\rangle - \mu. \tag{31}$$

As $\langle n_\sigma\rangle = 0.5$ and $\mu = U/2$, we have a situation like that for set I parameters.

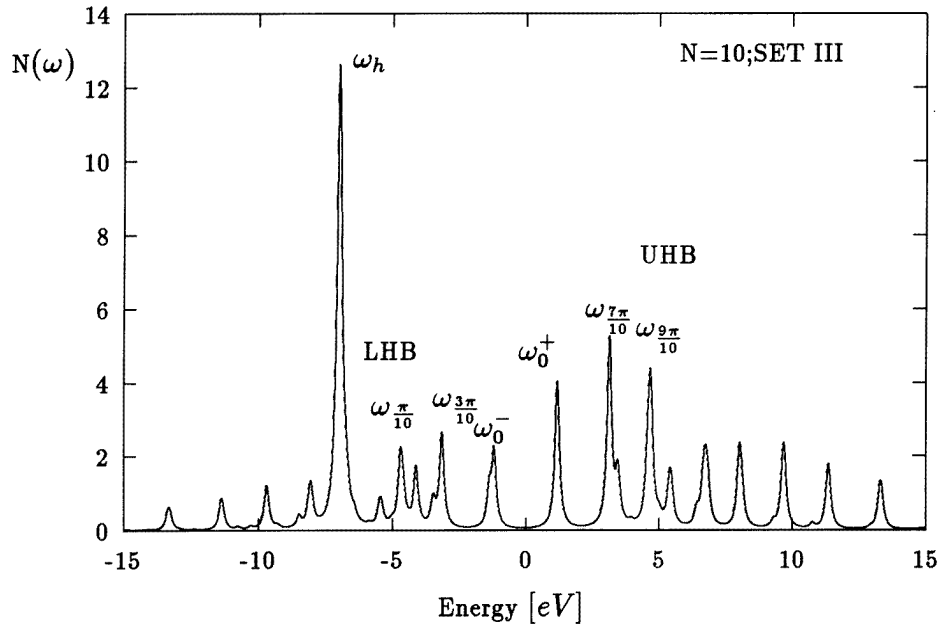

Figure 3. The spectral function $N(\omega) = N^E(-\omega) + N^A(\omega)$ for a 10-site cluster expressed in arbitrary units (set III parameters, ABC). The chemical potential $\mu = 1.18$ eV. The peak labels corresponding to different k-values were assigned using the HF approximation (see formula (31) and compare figure 1 assignments). The charge-transfer-type gap corresponds to a transition from a bonding ω_0^--state to an antibonding ω_0^+-state. The peak $\omega_h = -6.99$ eV (highest intensity) corresponds to promotion of an electron from a deep occupied to a shallow unoccupied level. We can identify the lower Hubbard band (LHB) and the upper Hubbard band (UHB) separated by the energy gap $E_{gap}^{10} = \omega_0^+ - \omega_0^- = 2.36$ eV $\simeq U/t$. Some peaks belong to higher subbands.

Looking at figure 3, where not the approximate (corresponding to formula (31)) but the computed (for the cluster) $N(\omega)$ is presented, we note the following.

(i) Coulomb interaction produces new states at around $\omega \simeq \pm U/2 = \pm 3.125$ eV corresponding to the lower hubbard band (LHB), the upper hubbard band (UHB) and to higher bands. This result (for large U) is a simple reproduction of similar earlier results (compare the numerical data of [44]).

(ii) The Coulomb interaction U opens a gap in the vicinity of Fermi energy. The gap can be estimated by using $E_{gap}^{10} = \omega_0^+ - \omega_0^- = 2.36 \pm 0.02$ eV (see figure 3; compare formula (31) and the discussion following figure 2).

(iii) There is a peak at the highest intensity: $\omega_h = -6.99$ eV. We note that the position of this peak is independent of the system size. Attempting to interpret ω_h, we observe that

the actual value of ω_h roughly corresponds to excitation of an electron from the bottom of the valence band to the lowest-lying level (degenerate) of the conduction band (the HF approximation). This peak corresponds to a transition from the $k = 0$ to the $k = \pm\pi/2$ level; it could be visible in x-ray photoemission (compare figure 6, later). This is a very simple interpretation. However, some other many-particle process might be responsible for ω_h.

Let us return to the problem of the LHB and the UHB. It is well known that for finite values of U/t the spectrum of the one-dimensional Hubbard Hamiltonian is separated into numerous disjoint subbands [12, 13]. (This holds also for large U [44, 45].)

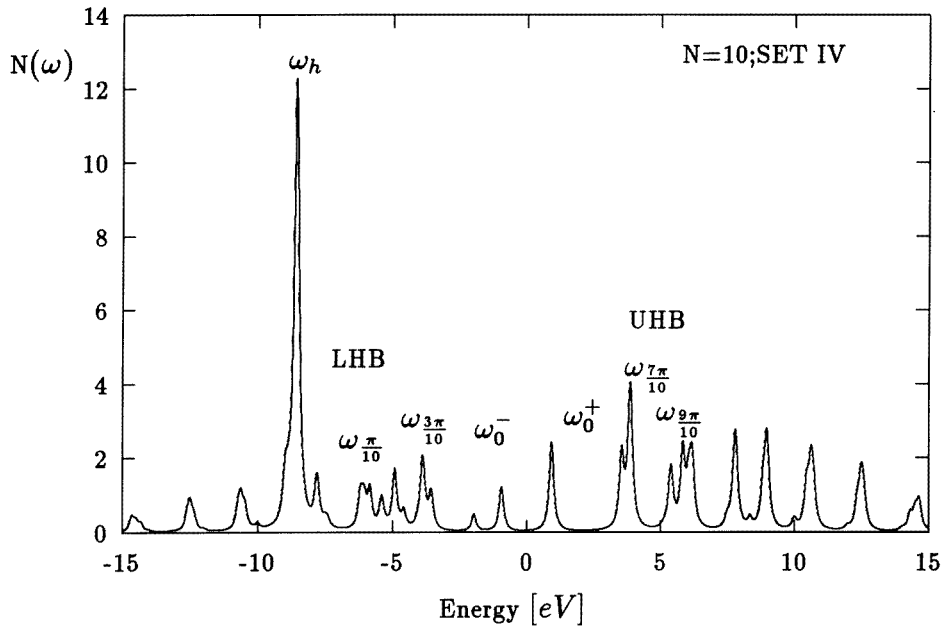

Figure 4. The spectral function $N(\omega) = N^E(-\omega) + N^A(\omega)$ for a 10-site cluster expressed in arbitrary units (set IV parameters, ABC). The chemical potential $\mu = 0.92$ eV. The intersite Coulomb interaction removes some degeneracies in the LHB and the UHB (splitting peaks for $\omega_{-7\pi/10}, \omega_{-9\pi/10}, \omega_{-3\pi/10}, \omega_{-\pi/10}$; compare figure 4 with figure 3) and moves the UHB (LHB) to higher (lower) energies. The charge-transfer-type gap corresponds to a transition from a bonding ω_0^--state to an antibonding ω_0^+-state. The peak $\omega_h = -8.57$ eV (highest intensity) is an analogue of the ω_h-peak from figure 3.

If E_l is the centre of gravity of the lth subband then the difference between two adjacent E_ls is U. To describe the motion of electrons in such a subband we define projection operators P_l. P_l projects out from a many-electron state particular configurations each of which contains l doubly occupied sites. Using a canonical transformation [46] the decomposed Hamiltonian is

$$H = \left(\sum_l P_l H \sum_l P_l\right) = H_0 + H_1 \tag{32}$$

$$H_0 = \sum_{l=0} P_l H P_l \tag{33}$$

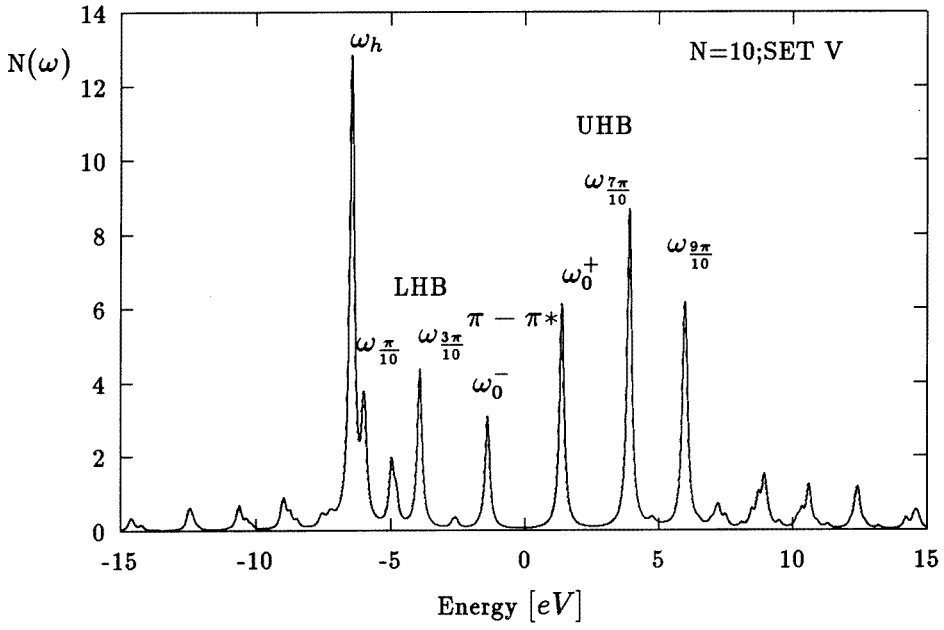

Figure 5. The spectral function $N(\omega) = N^E(-\omega) + N^A(\omega)$ for a 10-site cluster expressed in arbitrary units (set V parameters, ABC). The chemical potential $\mu = 1.41$ eV. The peak $\omega_h = -6.44$ eV (highest intensity) is an analogue of the ω_h-peaks from figures 3, 4. We can see a $\pi \rightarrow \pi^*$ charge-transfer-type gap corresponding to a transition from a bonding ω^--state to an antibonding ω^+-state ($E^{10}_{gap} = 2.82$ eV).

$$H_1 = \sum_{l=0} P_{l+1} H P_l + \sum_{l=0} P_{l-1} H P_l. \tag{34}$$

The terms $P_{l+1}HP_l$ ($P_{l-1}HP_l$) represent interband hopping from the lth to the $(l+1)$th ($(l-1)$th) subband. The effective Hamiltonian P_lHP_l describes the dynamical properties of an electron within a single lth subband.

On figure 3 we can identity: the LHB, the UHB, and some states which correspond to the next higher subband, i.e., P_0HP_0, P_1HP_1 and P_2HP_2. The subband centres are: $E_0 \simeq -U/2$, $E_1 \simeq U/2$, $E_2 \simeq \pm(E_1 + U/2)$, respectively.

The dominant peak in the LHB (labelled ω_h) corresponds to promotion of an electron from deep occupied to unoccupied levels.

For set IV parameters the Hamiltonian (1) becomes the extended Hubbard Hamiltonian. The corresponding density of states $N(\omega)$ is shown in figure 4.

When one makes a comparison with figure 3, one can notice the following features.

(i) The intersite Coulomb interaction removes some degeneracies in the LHB and UHB (splitting peaks for $\omega_{\pi/10}, \omega_{3\pi/10}, \omega_{7\pi/10}, \omega_{9\pi/10}$).

(ii) Peak ω_h shifts to lower energies (-8.57 eV). The interpretation of ω_h is identical to that in the case of the set III parameters model (see figure 6, later). It cannot be excluded that the mode ω_h may have some connection with the dimerization (the Peierls transition) (compare figure 6, later).

(iii) The UHB (LHB) moves a little to higher (lower) energies. The value of the shift depends on k (maximal for $k \simeq \pi$ and $k \simeq 0$, minimal for $k \simeq \pi/2$).

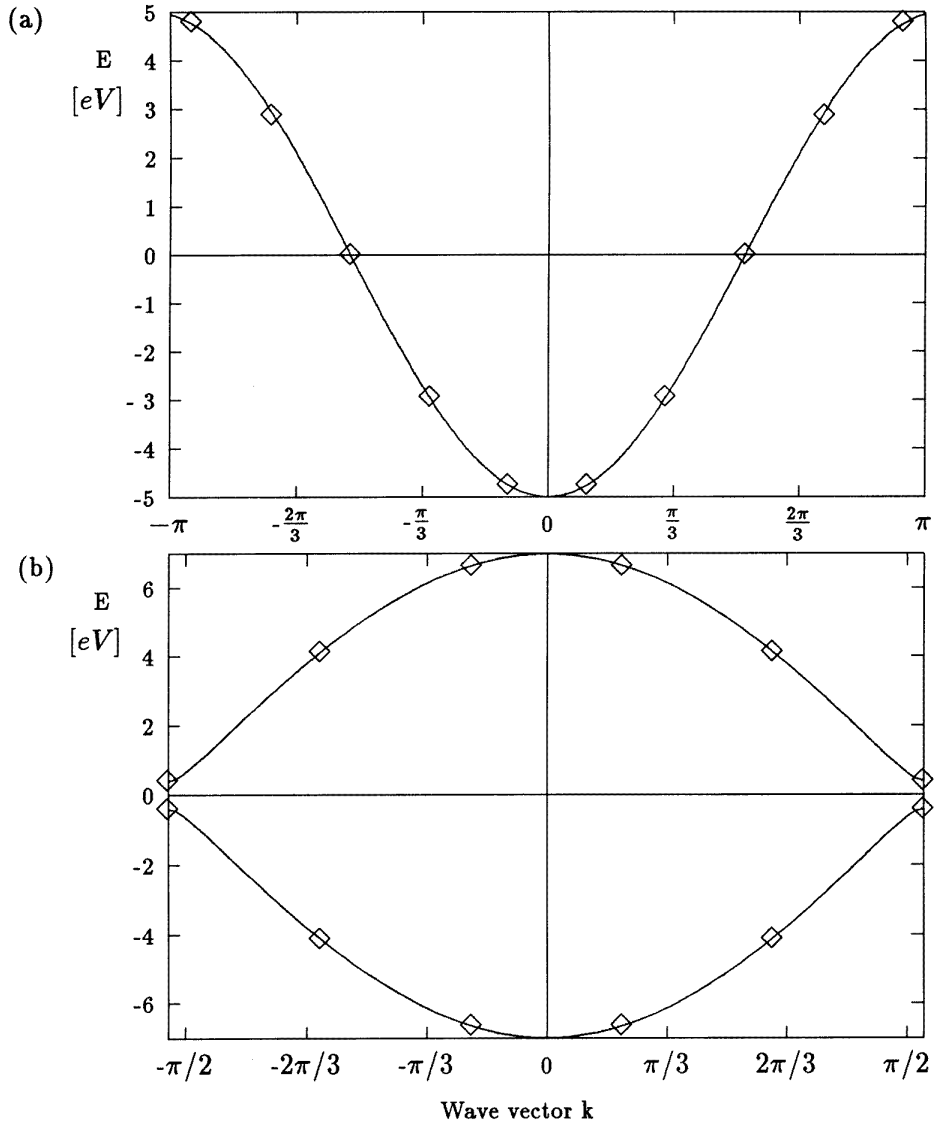

Figure 6. Valence band and conduction band energy levels in the HF approximation for an infinite system versus momentum. The actual values which would correspond to a 10-site system with antiperiodic boundary conditions are indicated as diamonds. (a) Upper panel. The model with set III parameters. The exact value of $\omega_h = -6.99$ eV for a 10-site cluster with ABC roughly corresponds to the excitation from the deepest ($k = 0$) valence band level to the lowest ($k = \pm\pi/2$) conduction band levels (-7.7 eV in the HF approximation). (b) Lower panel. The model with set V parameters. The exact value of $\omega_h = -6.44$ eV for a 10-site cluster with ABC roughly corresponds to the excitation from the deepest ($k = 0$) valence band level to the lowest ($k = \pm\pi/2$) conduction band levels (-7.06 eV in the HF approximation). The momentum axis is in the same units as the one for set III parameters (to make clear the Peierls transition from a single-unit undimerized chain to the double-unit dimerized one).

(iv) E_{gap} is smaller ($E^{10}_{gap} = \omega^{+}_{0} - \omega^{-}_{0} = 1.84 \pm 0.02$ eV).

These facts may be understood already at the level of HF approximation. Namely:

$$H_{HF} = \sum_{k,\sigma} \left(E^{N}_{k} + U\langle n_{\sigma}\rangle - \mu - \frac{V_k}{2}\mathcal{P}_{l,l+1} \right) c^{+}_{k,\sigma} c_{k,\sigma} \tag{35}$$

where $\mathcal{P}_{l,l+1}$ is the single-particle density matrix defined as $\mathcal{P}_{l,l+1} = \langle c^{+}_{l} c_{l+1}\rangle$ and V_k is the Fourier transform of V. The term $(V_k/2)\mathcal{P}_{l,l+1}$ can be included in an effective hopping integral [19] $t^{eff}_{l,l+1} = t_{l,l+1} - 0.5V\mathcal{P}_{l+1,l}$ leading to a model Hamiltonian like that described by equation (29) (the HF approximation, and set-III-type parameters corresponding to set IV parameters).

If the effective hopping integral is larger than $t_{l,l+1}$ (absolute values) then the energy of the excited states increases.

Figure 5 shows the density of states for set V (Coulomb interaction + dimerization).

We observe that:

(i) there is a large peak at the bottom of the LHB at the energy $\omega = -6.44$ eV $\simeq U$ of the same origin as those for the models with set III and set IV parameters (figure 6);

(ii) the intensity of the states for $|\omega| \geqslant 6$ eV is smaller than that corresponding to the cluster with set IV parameters;

(iii) the value E^{10}_{gap} is bigger ($E^{10}_{gap} = \omega^{+}_{0} - \omega^{-}_{0} = 2.82$ eV); the estimated value of E_{gap}, using the values E^{6}_{gap}, E^{8}_{gap} and E^{10}_{gap}, is found to be $E_{gap} = 1.55$ eV (set V—realistic parameters); the value of 1.55 eV is consistent within the estimation error with the experimental value of E^{exp}_{gap}.

These facts suggest that dimerization strongly influences the one-particle spectral function $N(\omega)$ (compare figure 5 and figure 4).

4. Summary

In this work we studied the Peierls Hubbard Hamiltonian for different sets of Hamiltonian parameters. We used the Lanczos method to calculate the ground-state properties and the single-particle spectral function $N(\omega)$. The analysis of the results leads to the following conclusions.

For all clusters the ground-state energy of the dimerized state is lower than the one obtained for the non-dimerized state.

From figures 1–5 or from the experimental data we can estimate E_{gap}. This is a very important fact because sometimes the exact solutions for Hamiltonian (1) are lacking and the computation of E_{gap} may prove difficult.

The Coulomb (U, V) and the electron–phonon interaction open a gap near the Fermi level. The estimated value of E_{gap} is 1.55 eV, which is close to the experimental value.

The Coulomb interaction produces new states as shown in figures 3 and 4. These states correspond to the UHB, the LHB and higher bands.

The electron–phonon interaction changes the spectrum:

(i) the value of E_{gap} increases (the increase is independent of the system size);

(ii) the intensities of the states for $|\omega| \geqslant 6$ eV decrease with respect to analogous intensities for clusters with set III or set IV parameters;

(iii) for set III–set V parameters we observe the intense peak labelled ω_h (at around $\omega \simeq U$) which corresponds to electron transition from occupied to unoccupied levels.

Let us note that many of the facts mentioned above may be already understood at the level of the HF approximation.

Acknowledgments

The authors are grateful to J Spałek and A M Oleś for fruitful discussions and many helpful comments. This work was supported by the Committee of Scientific Research (KBN) Project No 2PO3B 144 08.

Appendix A

For set II parameters the ground-state energy is [1, 18]

$$E_0^N(\zeta) = -N\frac{4t_0}{\pi}E(1-Z^2) + \frac{4t_0Z^2}{2\alpha^2} \tag{A1}$$

where $E(1-Z^2)$ is the complete elliptic integral of the second kind and $Z = 2\alpha\zeta/t_0$. For small z, equation (A1) becomes

$$E_0^N(\zeta) = -\frac{4t_0N}{\pi} - \frac{2t_0N}{\pi}\left[\ln\left(\frac{4}{|z|}\right) - \frac{1}{2}\right]z^2 + \frac{NKt_0Z^2}{2\alpha^2}. \tag{A2}$$

When the SSH model is extended by adding Coulomb interactions between electrons, then the change in the ground-state energy in the self-consistent-field approximation is [1]

$$\Delta E = -\frac{2NVz^2}{\pi^2}\ln^2\left(\frac{4}{|z|}\right). \tag{A3}$$

Adding (A3) to (A2) we obtain

$$E_0^N = -\frac{4t_0N}{\pi} + \left[\frac{Nt_0}{\pi} + \frac{Kt_0^2N}{2\alpha^2} - \frac{2t_0N}{\pi}\ln\left(\frac{4}{|z|}\right) - \frac{2NV}{\pi^2}\ln^2\left(\frac{4}{|z|}\right)\right]z^2. \tag{A4}$$

Comparing equation (A4) and equation (13) we obtain

$$\begin{aligned} e_0 &= -\frac{4t_0N}{\pi} \\ e_1 &= \frac{Nt_0}{\pi} + \frac{Kt_0^2N}{2\alpha^2} \end{aligned} \tag{A5}$$

$$\begin{aligned} e_2 &= -\frac{2t_0N}{\pi} \\ e_3 &= -\frac{2NV}{\pi^2}. \end{aligned} \tag{A6}$$

We note that within this approximation the ground-state energy does not depend on U.

References

[1] Heeger A J, Kivelson S, Schrieffer J R and Su W P 1988 *Rev. Mod. Phys.* **60** 781
[2] Fulde P 1995 *Electron Correlation in Molecules and Solids (Springer Series in Solid-State Sciences)* (Berlin: Springer)
[3] Borrman W and Fulde P 1986 *Europhys. Lett.* **2** 471
[4] Horsch S, Horsch P and Fulde P 1983 *Phys. Rev.* B **28** 5977
[5] Horsch S, Horsch P and Fulde P 1984 *Phys. Rev.* B **29** 1870
[6] Bormann W and Fulde P 1987 *Phys. Rev.* B **35** 9569

[7] Kőnig G and Stollhoff G 1990 *Phys. Rev. Lett.* **65** 1239; 1990 *J. Chem. Phys.* **91** 2993
[8] Waas V, Buttner H and Voit J 1990 *Phys. Rev.* B **41** 9366
[9] Rościszewski K and Oleś B 1993 *J. Phys.: Condens. Matter* **5** 7289
[10] Hubbard J 1963 *Proc. R. Soc.* A **276** 238
[11] Hubbard J 1964 *Proc. R. Soc.* A **281** 401
[12] Cabib D and Callen E 1973 *Phys. Rev.* B **12** 55 249
[13] Wolf V 1983 *Nucl. Phys.* B **255** 391
[14] Hirsch J E 1980 *Phys. Rev.* B **22** 5259
[15] Fourcade B and Sproken G 1984 *Phys. Rev.* B **29** 5089
[16] Fourcade B and Sproken G 1984 *Phys. Rev.* B **29** 5096
[17] Van Dongen P G J 1991 *Phys. Rev. Lett.* **67** 757
[18] Su W P, Schrieffer J R and Heeger A J 1980 *Phys. Rev.* B **22** 2099
[19] Horsch P 1981 *Phys. Rev.* B **24** 7351
[20] Nishino T 1992 *Electron Correlation Effects in Low Dimensional Periodic Systems (Osaka, 1992); J. Phys. Soc. Japan* **61** 3651
[21] Kehlert H, Leitner O and Leising G 1989 *Synth. Met.* **17** 467
[22] Baeriswyl D, Campbell D K and Mazumdar S 1990 An overview of the theory of π-conjugated polymers *Los Alamos Report* LA-UR 90-826
[23] 1991 *International Winter School on Electronic Properties of Polymers (Kirchberg, Tirol, Austria, 1991) (Springer Series in Solid-State Sciences 107)* (Berlin: Springer)
[24] Gammel J T, Campbell D K, Mazumdar S and Loh E Y 1991 *Synth. Met.* **43** 3471
[25] Jullen R and Martin R M 1982 *Phys. Rev.* B **26** 6173
[26] Lanczos C 1950 *J. Res. NBS* **45** 255
[27] Ralston A 1985 *A First Course in Numerical Analysis* (New York: McGraw-Hill)
[28] Loh E Y Jr, Campbell D K and Tinka Gammel J 1988 *Lanczos Diagonalizations of the 1-D Peierls–Hubbard Model (NATO ASI Series B: Physics, vol 213)*
[29] Lin H Q and Gubernatis J E 1993 *Comput. Phys.* **7** 400
[30] Gagliano E R and Balseiro C A 1987 *Phys. Rev.* B **38** 11 766
[31] Gagliano E R and Balseiro C A 1987 *Phys. Rev.* B **59** 2999
[32] Heine V 1980 *Solid State Physics* vol 35 (New York: Academic) p 1
[33] Lieb E H and Mattis D 1962 *Phys. Rev.* **125** 164
[34] Lieb E H and Wu F Y 1968 *Phys. Rev. Lett.* **20** 1445
[35] Ruckenstein A E, Hirschfeld P and Appel J 1987 *Phys. Rev.* B **36** 973
[36] Soos Z G and Ramasesha S 1984 *Phys. Rev.* B **29** 5410
[37] Hirsch J E 1984 *Phys. Rev. Lett.* **53** 2327
[38] Baeriswyl D and Maki K 1985 *Phys. Rev.* B **31** 6633
[39] Muller-Hartman E 1989 *Z. Phys.* B **76** 211
[40] Muller-Hartman E 1989 *Z. Phys.* B **74** 507
[41] Liegener C M 1988 *J. Chem. Phys.* **88** 6999
[42] Zheng H 1994 *Phys. Rev.* B **50** 6717
[43] Paraschik D Yu, Kulakov A T and Kobryanskii V M 1994 *Phys. Rev.* B **50** 907
[44] Eskes H, Meinders M B J and Sawatzky G A 1991 *Phys. Rev. Lett.* **67** 1035
[45] Meinders M B J, Eskes H and Sawatzky G A 1993 *Phys. Rev.* B **48** 3916
[46] Chao K A, Spałek J and Oleś A M 1978 *Phys. Rev.* B **18** 3453